Design and Performance Estimation of a 20 T 46 mm No-Insulation All-REBCO User Magnet

Kwangmin Kim, Kabindra Bhattarai, Kwang Lok Kim, Hongyu Bai, Iain R. Dixon, *Senior Member, IEEE*, Thomas A. Painter, *Member, IEEE*, Uijong Bong, David C. Larbalestier, *Fellow, IEEE*, and Seungyong Hahn

***Abstract*—This paper reports on a proposed design and estimation of performance of a 20 T no-insulation (NI) high temperature superconductor (HTS) standalone user magnet for the National High Magnetic Field Laboratory. It consists of a stack of 18 double pancake coils wound with REBCO tapes from two different vendors, SuNAM and SuperPower, chosen for their complementary in-field critical current, mechanical properties and cost properties. The inner and outer winding diameters and overall height of the magnet are 46 mm, 102.6 mm, and 163.4 mm, respectively. The magnet is designed to generate a 20 T central field at its nominal operating current of 316 A in liquid helium at 4.2 K. The inductance and stored energy are 1.89 H and 94.4 kJ, respectively. In addition to the detailed design parameters, this paper presents a stress analysis, NI charging analysis and post-quench analysis, followed by discussion of design parameters and estimated performance of the proposed 20 T NI HTS magnet.**

***Index Terms*—high temperature superconductors, no-insulation, quench, REBCO magnet, stress.**

I. Introduction

THE no-insulation (NI) winding technique has been proven to provide a practical and easy solution for the high temperature superconductor (HTS) magnet protection and stability. Since it was first proposed at MIT in 2010 [1], significant progress has been made in NI REBCO magnet technology. Notable milestones include: (1) an 18 T, 70 mm bore, all-REBCO NI magnet, designed and constructed by a collaboration between SuNAM and Seoul National University, which represents the NI user magnet operating over 2 years [2]; (2) a 32.5 T field generation with 14.5 T metal-as-insulation HTS coil by Commissariat à l'Energie Atomique et aux énergies alternatives (CEA) and Laboratoire National des Champs Magnétiques Intenses (LNCMI) [3]; (3) 32.35 T fully superconducting magnet that was designed and constructed by the Institute of Electrical Engineering (IEE), Chinese Academy of Sciences (CAS) [4]; (4) a 14.4 T 14 mm NI REBCO insert that successfully generated a total combined field of 45.5 T (record high DC field) in a 37 mm bore of the 31.1 T resistive magnet at the National High Magnetic Field Laboratory (NHMFL) [5]; even more NI REBCO magnets are being researched and developed continuously [6]–[12]. The results have demonstrated a strong potential of the NI-REBCO magnet technology for the next generation of high field magnets. Motivated by the recent achievements, a project to design, construct, and operate a 20 T 46 mm no-insulation all-REBCO user magnet was launched at the NHMFL.

This paper reports on the design and performance estimation of the 20 T magnet, hereinafter named 'NI20T'. The magnet was designed to satisfy the following design factors: (1) a 20 T center field with $\leq$0.05% field homogeneity over a 1 cm diameter spherical volume (DSV); (2) $\geq$34 mm diameter cold bore; (3) $\leq$1 hour charging time to reach the maximum field; (4) attain 99% of target field within 5 minutes after reaching the target current; (5) $\geq$25% critical current (I_c) margin; and (6) $\leq$0.5% hoop strain of double pancake (DP) coils during quench.

First, we report key design parameters followed by numerical simulation results of: (1) magnetic field and stress analyses; (2) NI charging behavior and estimation of liquid helium consumption; and (3) quench behavior including non-uniform current distribution, peak stress (with strain), and local temperature rise.

II. Magnet Design

A. Key Parameters of NI20T

Table I shows the key parameters of NI20T. In order to achieve the target I_c margin and to avoid high induced current at the mid-section during the quench, two REBCO tapes having different performances were considered. The contact surface resistance (R_{ct}) of each vendor's REBCO tape was measured through individual experiments to estimate the charging behavior of the NI20T. Fig. 1(a) shows the configuration of NI20T. A total of 18 DP coils are designed to be wound with SuNAM and SuperPower RECBO tapes using the so-called "multi-width" concept [13]. In Table I, we define a "module" as a group of DP

Manuscript received September 24, 2019; accepted February 4, 2020. Date of publication February 20, 2020; date of current version March 25, 2020. This work was supported in part by the National High Magnetic Field Laboratory, which is supported by National Science Foundation (NSF) Cooperative Agreement DMR-1644779 and in part by the State of Florida. The work of U. Bong and S. Hahn was supported by the National Research Foundation of Korea as a part of Mid-Career Research Program under Grant 2018R1A2B3009249. *(Corresponding author: Seungyong Hahn.)*

Kwangmin Kim, Kwang Lok Kim, Hongyu Bai, Iain R. Dixon, Thomas A. Painter, and David C. Larbalestier are with the National High Magnetic Field Laboratory, Florida State University, Tallahassee, FL 32310 USA (e-mail: kwangmin.kim@asc.magnet.fsu.edu).

Kabindra Bhattarai was with the NHMFL, FSU, Tallahassee, FL 32310 USA. He is now with the GE Healthcare, Florence, SC 29501 USA (e-mail: krb15d@my.fsu.edu).

Uijong Bong and Seungyong Hahn are with the Department of Electrical and Computer Engineering, Seoul National University, Seoul 08826, South Korea (e-mail: hahnsy@snu.ac.kr).

Color versions of one or more of the figures in this article are available online at https://ieeexplore.ieee.org.

Digital Object Identifier 10.1109/TASC.2020.2975166

TABLE I
KEY PARAMETERS OF NI20T

Parameter	Module 1	Module 2	Module 3
Magnet configuration			
Manufacturer	SuNAM	SuperPower	
Width; thickness [mm]	4.1; 0.12	4.1; 0.096	6.1; 0.096
Substrate thickness [mm]	0.1	0.05	0.05
Cu stabilizer thickness [μm]	7.5 (per side)	20 (per side)	20 (per side)
Equivalent Young's modulus (E_r, E_h, E_z) [GPa]	107; 168; 168	72; 130; 130	
Equivalent Poisson's ratio (ν_{rh}, ν_{hz}, ν_{rz})	0.21; 0.33; 0.21	0.18; 0.33; 0.18	
Inner diameter [mm]	46		
Outer diameter [mm]	102.6		
Overall height [mm]	163.4		
Turns per pancake	236	295	
Conductor per DP [m]	110.2	138.0	
Estimated R_c [mΩ]	9.5[a], 47.3[b]		
Operation			
Center field [A]	20		
Operating current, I_{op} [A]	316		
Conductor current density [A/mm^2]	642.3	802.8	539.6
Inductance [H]	1.89		
Storage energy at I_{op} [kJ]	94.4		
Estimated time constant, τ [sec]	198.9[a], 40.0[b]		
Operating temperature, T_{op} [K]	4.2		

Contact surface resistance: [a] $R_{ct} = 10\ \mu\Omega{\cdot}\text{cm}^2$, [b] $R_{ct} = 50\ \mu\Omega{\cdot}\text{cm}^2$

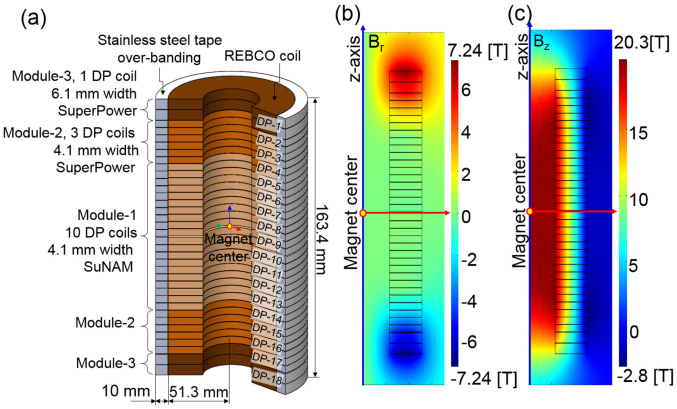

Fig. 1. Configuration and magnetic field distribution of NI20T; (a) to-scale drawing, (b) radial direction magnetic field, and (c) axial direction magnetic field.

coils wound with REBCO tape of the width and same vendor. Module-1 is located at the magnet center and consists of 10 DP coils wound with 4.1 mm wide SuNAM REBCO tape, while modules-2 and 3 are made of SuperPower tapes, 4.1 mm and 6.1 mm wide, respectively. 0.2 mm thick G10 spacers were used for pancake-to-pancake insulation, and 1 mm thickness spacers were placed between center DP coils (DP9 and DP10) to achieve the target field homogeneity.

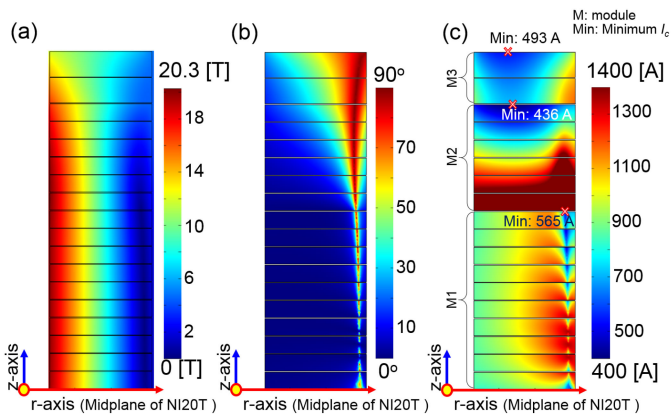

Fig. 2. Critical current estimation of NI20T; (a) normal field distribution, (b) field angle (θ) distribution, and (c) critical current distribution.

B. Electromagnetic Analysis and I_c Estimation Based on the Angular Dependence of NI20T

Fig. 1(b) and (c) show the magnetic field distribution of the NI20T. The magnet generates 20 T center field at the nominal operating current of 316 A, the overall current density (J_e) of modules-1, 2, and 3 are 642, 803, and 540 A/mm^2, respectively. The peak radial field of 7.2 T was found in the outer module-3 made with 6.1 mm wide SuperPower tape. The calculated axial direction magnetic field (B_z) and radial direction magnetic field (B_r) homogeneities over the 1 cm DSV are 0.022% and -0.012%, respectively.

The in-field characteristics of both SuNAM and SuperPower REBCO tapes were measured in liquid helium at 4.2 K at various external magnetic fields. The tape's angular dependency was taken into account to estimate the I_c values based on the fit-function developed [14], [15].

Fig. 2 shows simulation results of: (a) magnitude of magnetic field (B_{norm}); (b) field angle (θ), where "90-degree" is defined as field parallel to the c-axis of REBCO; and (c) estimated critical current (I_c) in consideration of B_{norm}, θ, and tape width at 4.2 K. The minimum I_c of modules 1, 2 and 3 are calculated to be 565 A, 436 A and 493 A, respectively. Thus, NI20T operated at 316 A has $\sim$28% I_c margin.

C. Mechanical Characteristics of NI20T

Since NI20T is expected to be "dry-wound" without epoxy, the so-called "self-supporting-turn" characteristic of NI20T is used for the stress analysis. The equivalent orthotropic Young's modulus and Poisson's ratios were calculated using the mixture rule for stress analysis [16], [17]. Stainless steel over banding with a total radial build of 10 mm is designed to be wound over each DP coil to reduce the hoop strain during quench. The considered Young's modulus and Poisson ratios of the stainless steel over banding are 195 GPa and 0.33%, respectively [18].

Fig. 3 shows the calculation results of stress and strain of NI20T. To calculate mechanical characteristics of NI20T, force equilibrium and generalized Hooke's laws were used [18]. The analysis predicts a calculated peak magnetic hoop stress of

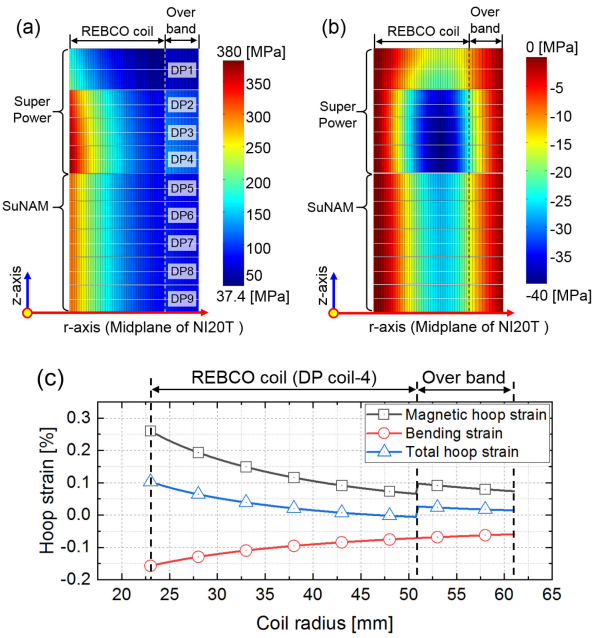

Fig. 3. Mechanical simulation results of upper-half of NI20T: (a) Magnetic hoop stress; (b) magnetic radial stress; and (c) overall strains including magnetic and bending strains on axial mid-plane of DP4.

380 MPa at DP4. The peak magnetic hoop strain and bending strain are 0.26% (at r: 23 mm, z: 47.6 mm) and −0.16% (at r: 23 mm, z: 47.6 mm), respectively. Provided that NI20T is wound with the REBCO layer facing inward to develop significant compressive bending strain, the overall hoop strain is estimated to be compressive. Under this assumption, the peak strain (hoop + bending) is estimated to be 0.1% (at *r:* 23 mm, z: 47.6 mm), still acceptable for the 95% I_c retention strain of 0.5% [19], [20].

III. Performance Estimation of NI20T

A. Charging Behavior of NI20T

Charging delay is an innate demerit of an NI magnet due to the bypass current between turns. We estimated the charging behavior of NI20T using the lumped circuit model [21]. Previous NI coil test results confirmed the increase in $R_{\rm ct}$ upon the charging-discharging cycles on the NI coils [22].

Therefore, we investigated the charging behavior of NI20T using two different R_{ct} values which were obtained from earlier experimental results (10 $\mu\Omega{\cdot}\text{cm}^2$, 50 $\mu\Omega{\cdot}\text{cm}^2$) [5], [22]. The calculated values of R_c of NI20T are 9.5 mΩ and 47.3 mΩ. Fig. 4 shows the estimated charging profiles of NI20T for both R_c conditions. At a constant ramp rate of $dI_{ps}/dt = 0.2$ A/sec, the durations to reach the 99.9% of expected magnetic field at the power supply current of 316 A were calculated to be ≈16.1 minutes at $R_{\rm ct}$ = 10 $\mu\Omega{\cdot}\text{cm}^2$ and ≈2.2 minutes at $R_{\rm ct}$ = 50 $\mu\Omega{\cdot}\text{cm}^2$, respectively. The NI20T shows lower charging loss results when the R_{ct} value was 50 $\mu\Omega{\cdot}\text{cm}^2$ than the value of 10 $\mu\Omega{\cdot}\text{cm}^2$. During the whole charging process, Joule heating due to the turn-to-turn leakage current was estimated to be 3 W, which corresponds to a total energy dissipation of 4.7 kJ, translating into 1.8 liter of liquid helium consumption

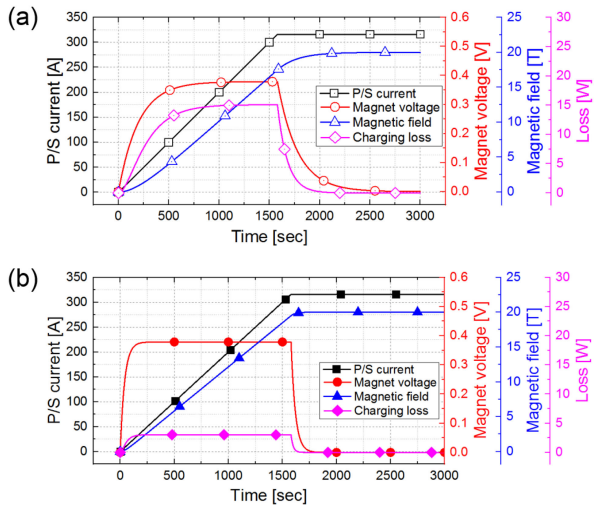

Fig. 4. Charging profile of NI20T with 0.2 A/s ramping rate: (a) $R_{\rm ct}$ = 10 $\mu\Omega{\cdot}\text{cm}^2$; (b) $R_{\rm ct}$ = 50 $\mu\Omega{\cdot}\text{cm}^2$.

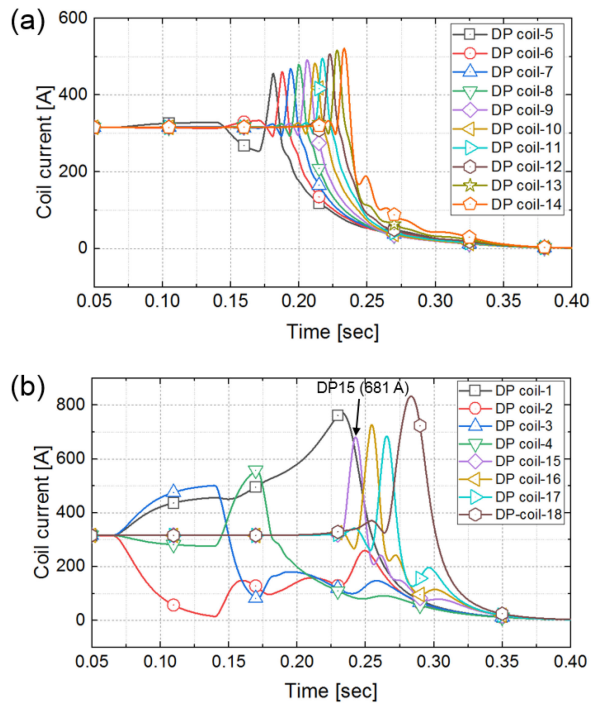

Fig. 5. Azimuthal current pattern of each DP coil during NI20T quench; (a) module-1 (SuNAM), (b) module-2 (SuperPower).

at $R_{\rm ct}$ = 50 $\mu\Omega{\cdot}\text{cm}^2$. For more precise field control during ramping and even in steady-state operation, we are considering active-feedback control, whose validity was reported previously [23].

B. Post-Quench Behavior of NI20T

The most updated in-house simulation code based on the lumped circuit model was adopted for quench analysis of NI20T [24], [25]. Fig. 5 shows the respective azimuthal current pattern and temperature variation of each DP coil during the NI20T quench considering R_{ct} of 50 $\mu\Omega{\cdot}\text{cm}^2$. Quench was assumed to

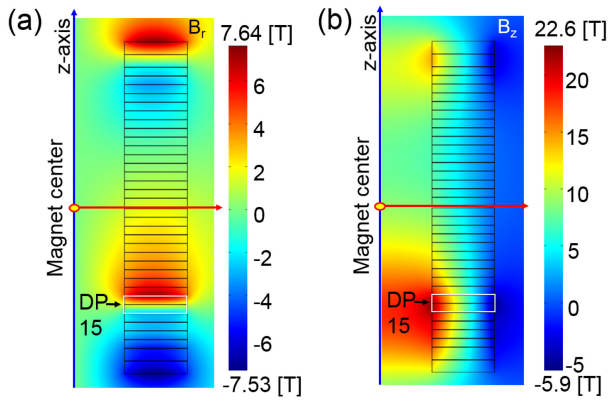

Fig. 6. Unbalanced magnet field distribution of NI20T during quench; (a) radial direction magnetic field, (b) axial direction magnetic field.

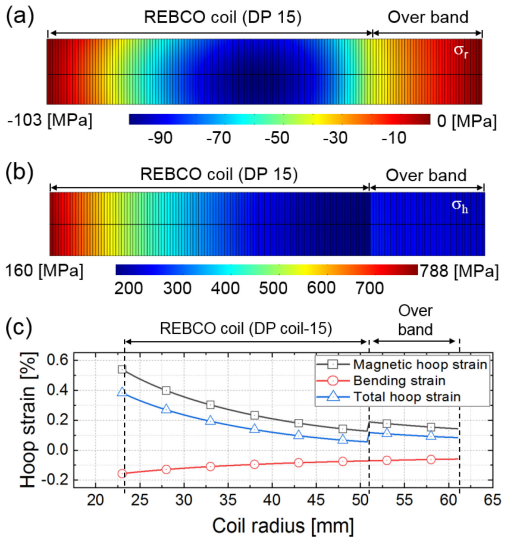

Fig. 7. Mechanical simulation results of DP15 during quench; (a) radial stress distribution, (b) hoop stress distribution, and (c) overall calculated strains on axial midplane of DP15.

be initiated at the operating current of 316 A from DP2 which has the lowest I_c margin. As seen in Fig. 5, DP2 current starts decreasing immediately after the quench and the rest of DPs responded due to the electromagnetic coupling. Mutual coupling causes the current in adjacent pancakes to rise to its critical current, initiating quench reduction of current and initiation of quench in the next DP. This "fast electromagnetic quench propagation" is a unique characteristic of an NI magnet that makes it quite distinguishable from its conventional insulated counterpart. Our model predicts that the quench propagates to all pancake coils in ∼0.32 s. During the quench propagation, some DPs experience overcurrent as seen in Fig. 5. The peak current was calculated to be 830 A in DP18 at $t = 0.28$ s.

The NI magnet experiences huge stress due to the large induced current during quench [26], [27]. Therefore, we investigated peak stress and strain of NI20T. The stress and strain were calculated based on the azimuthal current and unbalanced field distribution of the NI20T. Fig. 5 shows that DP18 has the peak azimuthal current, but the highest magnetic hoop stress was

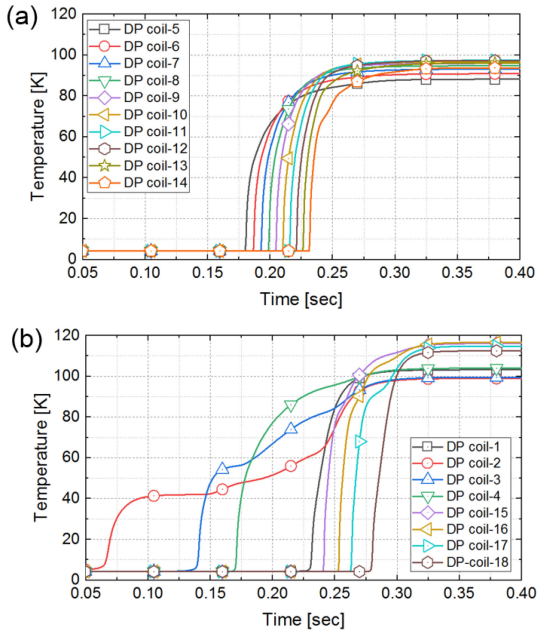

Fig. 8. Temperature variation of each DP coil during NI20T quench; (a) module-1, (b) module-2 and 3.

observed in DP15 through mechanical simulation (at 0.24 s). Fig. 6 shows the unbalanced field distribution of NI20T at quench moment which showed the peak stress.

The highest B_z field was generated around DP15. Fig. 7 shows the generated peak stress and overall strain of DP15 during the quench. The calculated peak magnetic hoop stress and strain are 788 MPa and 0.54%, respectively. The total hoop strain considering the bending strain (−0.16%) is 0.38%.

Fig. 8 shows the temperature profiles of each DP coil during the quench. Final temperatures of DP coils of NI20T were calculated to be 117 K (DP16) and 88 K (DP5), respectively. The average final temperature of NI20T is 99 K. The final temperatures of the end DP coils (module-2 and 3) are larger than those of the central DP coils in module-1, indicating that a larger amount of energy is dissipated in the end DP coils.

IV. Conclusion

This paper reports the design and performance estimate of a 20 T 46 mm winding diameter, all-REBCO NI magnet. It consists of a stack of 18 DP coils wound with tapes from two different vendors (SuNAM and SuperPower). The inner radius, outer radius and height of the magnet are 46 mm, 51.3 mm, and 163.4 mm, respectively. The magnet generates a center field of 20 T at an operating current of 316 A in a bath of liquid helium at 4.2 K. With an inductance of 1.89 H, the stored energy at its nominal operation is 94.4 kJ. Each module has ∼28% critical current (I_c) margin and the angular dependence of the tape's critical current was considered. The post-quench simulation using the lumped circuit model showed a peak temperature of 117 K. The calculated peak magnetic hoop stress of NI20T is 380 MPa (at DP4) during normal operation. The predicted peak magnetic hoop stress and hoop strain of DP15 were 788 MPa and 0.38%, respectively during the quench.

REFERENCES

[1] S. Hahn, D. K. Park, J. Bascuñán, and Y. Iwasa, "HTS pancake coils without turn-to-turn insulation," *IEEE Trans. Appl. Supercond.*, vol. 21, no. 3, pp. 1592–1595, Jun. 2011.

[2] J. Kim *et al.*, "Design, fabrication, and test results of an 18 T GdBCO magnet for axion detectior," in *Proc. 25th Int. Conf. Magnet Technol.*, Amsterdam, The Netherlands, 2017.

[3] J. B. Song, X. Chaud, F. Debray, P. Fazilleau, and T. Lécrevisse, "The high field HTS insert nougat reached a record field of 32.5 T," Accessed on: Jan. 7, 2020. [Online]. Available: http://srv-web.lncmi.cnrs.fr/actualite/the-high-field-hts-insert-nougat-reached-a-record-field-of-32-5-t/

[4] Chinese Academy of Sciences (CAS), "Scientists develop world-record 32.35 tesla with an all-superconducting magnet," Accessed on: Dec. 9, 2019. [Online]. Available: http://english.cas.cn/newsroom/research_news/tech/201912/t20191209_227468.shtml

[5] S. Hahn *et al.*, "45.5-tesla direct-current magnetic field generated with a high-temperature superconducting magnet," *Nature*, vol. 570, pp. 496–449, 2019.

[6] S. Yoon, J. Kim, K. Cheon, H. Lee, S. Hahn, and S. H. Moon, "26T 35 mm all-$GdBa_2Cu_3O_{7-x}$ multi-width no-insulation superconducting magnet," *Supercond. Sci. Technol.*, vol. 29, 2016, Art. no. 04LT04.

[7] J. Choi *et al.*, "Commercial design and operating characteristics of a 300 kW superconducting induction heater (SIH) based on HTS magnets," *IEEE Trans. Appl. Supercond.*, vol. 29, no. 5, Aug. 2019, Art. no. 3700105.

[8] J. B. Song, X. Chaud, B. Borgnic, F. Debray, P. Fazilleau, and T. Lecrevisse, "Construction and test of a 7 T metal-as-insulation HTS insert under a 20 T high background magnetic field at 4.2 K," *IEEE Trans. Appl. Supercond.*, vol. 29, no. 5, Aug. 2019, Art. no. 4601705.

[9] J. Liu, L. Wang, L. Qin, Q. Wang, and Y. Dai, "Recent development of the 25 T all-superconducting magnet at IEE," *IEEE Trans. Appl. Supercond.*, vol. 28, no. 4, Jun. 2018, Art. no. 4301305.

[10] Y. Suetomi, S. Takahashi, T. Takao, H. Maeda, and Y. Yanagisawa, "A novel winding method for a no-insulation layer-wound REBCO coil to provide a short magnetic field delay and self-protect characteristics," *Supercond. Sci. Technol.*, vol. 32, 2016, Art. no. 045003.

[11] R. Gupta *et al.*, "Status of the 25 T, 100 mm bore HTS solenoid for an axion dark matter search experiment," *IEEE Trans. Appl. Supercond.*, vol. 29, no. 5, Aug. 2019, Art. no. 4602105.

[12] C. Barth *et al.*, "Generation of 25 T with an all-superconducting magnet system: Field profile and field quality measurements of a layer-wound 4 T REBCO insert coil for a 21 T LTS magnet," *Supercond. Sci. Technol.*, vol. 32, 2019, Art. no. 075005.

[13] S. Hahn *et al.*, "No-insulation multi-width winding technique for high temperature superconducting magnet," *Appl. Phys. Lett.*, vol. 130, 2013, Art. no. 173511.

[14] J. Šouc, E. Pardo, M. Vojenčiak, and F. Gömöry, "Theoretical and experimental study of AC loss in high temperature superconductor single pancake coils," *Supercond. Sci. Technol.*, vol. 22, 2009, Art. no. 015006.

[15] D. K. Hilton, A. V. Gavrilin, and U. P. Trociewitz, "Practical fit functions for transport critical current versus field magnitude and angle data from (RE)BCO coated conductors at fixed low temperatures and in high magnetic fields," *Supercond. Sci. Technol.*, vol. 28, 2015, Art. no. 074002.

[16] C. C. Clicknera *et al.*, "Mechanical properties of pure Ni and Ni-alloy substrate materials for Y–Ba–Cu–O coated superconductors," *Cryogenics*, vol. 46, p. 432–438, 2006.

[17] J. Lu, E. S. Choi, and H. D. Zhou, "Physical properties of Hastelloy C-276^{TM} at cryogenic temperatures," *J. Appl. Phys.*, vol. 103, 2008, Art. no. 064908.

[18] Y. Iwasa, *Case Studies in Superconducting Magnet*, 2nd ed. New York, NY, USA: Springer, 2009.

[19] H. S. Shin, M. J. Dedicatoria, S. Awaji, and K. Watanabe, "Characteristic strain response of I_c in SmBCO coated conductor tapes under magnetic field at 77 K," *IEEE Trans. Appl. Supercond.*, vol. 22, no. 3, Jun. 2012, Art. no. 6600404.

[20] H. S. Shin and M. J. Dedicatoria, "Intrinsic strain effect on critical current in Cu-stabilized GdBCO coated conductor tapes with different substrates," *Supercond. Sci. Technol.*, vol. 26, 2013, Art. no. 0550055.

[21] X. Wang *et al.*, "Turn-to-turn contact characteristics for an equivalent circuit model of no-insulation ReBCO pancake coil," *Supercond. Sci. Technol.*, vol. 26, 2013, Art. no. 035012.

[22] T. Painter *et al.*, "Design, construction, and operation of a 13 T 50 mm no-insulation REBCO insert for a 20 T all-superconducting user magnet," in *Proc. 26th Int. Conf. Magnet Technol.*, Amsterdam, The Netherlands, 2017.

[23] S. Kim, S. Hahn, K. Kim, and D. Larbalestier, "Method for generating linear current-field characteristics and eliminating charging delay in no-insulation superconducting magnets," *Supercond. Sci. Technol.*, vol. 30, 2017, Art. no. 035020.

[24] K. R. Bhattarai, K. Kim, S. Kim, S. G. Lee, and S. Hahn, "Quench analysis of a multiwidth no-insulation 7-T 78-mm REBCO magnet," *IEEE Trans. Appl. Supercond.*, vol. 27, no. 4, Jun. 2017, Art. no. 4603505.

[25] K. R. Bhattarai *et al.*, "Understanding quench in no-insulation (NI) REBCO magnets through experiments and simulations," *Supercond. Sci. Technol.*, vol. 33, 2020, Art. no. 035002.

[26] W. D. Markiewicz, T. Painter, I. Dixon, and M. Bird, "Quench transient current and quench propagation limit in pancake wound REBCO coils as a function of contact resistance, critical current, and coil size," *Supercond. Sci. Technol.*, vol. 32, 2019, Art. no. 105010.

[27] S. Noguchi *et al.*, "Quench analyses of the MIT 1.3-GHz LTS/HTS NMR magnet," *IEEE Trans. Appl. Supercond.*, vol. 29, no. 5, Aug. 2019, Art. no. 4301005.